JOURNAL OF SPACECRAFT AND ROCKETS
Vol. 37, No. 2, March–April 2000

Computational Heat-Transfer Modeling of Thermal Energy Storage Canisters for Space Applications

Pavel Sokolov* and Mounir Ibrahim†
Cleveland State University, Cleveland, Ohio 44115-2425
and
Thomas Kerslake‡
NASA John H. Glenn Research Center at Lewis Field, Cleveland, Ohio 44135

A computer code has been developed for analyzing the phenomena occurring in cylindrical metal canisters containing a high-temperature phase change material. Such canisters are normally used as thermal storage elements in heat receivers of solar dynamic power systems for low-orbit space vehicles. The code is a useful canister design tool and able to predict the temperature distributions and the void behavior in the canisters. These in turn are used for the canister thermal stress analyses. The emphasis in the development of the code has been made on accurate descriptions of the solid-liquid phase change process, void dynamics and heat transfer, convective and radiative heat-transfer modes in the phase change material. The abilities of the code include computations of three-dimensional and axisymmetric heat transfer and fluid mechanics phenomena inside the canisters. The code validation has been made based on the results of ground tests and two thermal energy storage flight experiments. The validated code has been used for canister analyses. The following features have been examined: 1) the location of hot spots in the canister, especially canister walls; 2) the void location and heat-transfer predictions; 3) the importance of radiative and convective heat-transfer modes in the void and liquid phase change material; and 4) the influence of three-dimensional vs axisymmetric boundary conditions on the canister performance.

Nomenclature

A = surface area
c = thermal capacity
D_c = directional cosine
E = energy
e = enthalpy
H_m = phase change material (PCM) heat of fusion
h = heat-transfer coefficient
I = radiative intensity
I_b = black-body intensity
k = thermal conductivity
m = mass
Nu = Nusselt number
q = heat flux
r = radial coordinate
$\boldsymbol{r}$ = position vector
S = radiative source function
S_m = modified radiative source function
$\boldsymbol{s}$ = direction vector
T = temperature
T_f = cooling fluid temperature
T_m = PCM melting point
t = time
V = volume
$\boldsymbol{v}$ = velocity in the liquid PCM
x_f = liquid PCM mass fraction (PCM quality) $= e/H_m$
z = axial coordinate
z_{rad} = z coordinate of the radiator emitting surface
α = absorption coefficient
β = extinction coefficient
β_m = modified extinction coefficient
ΔV = finite volume
Δz = size of the z grid
ε = emissivity
θ = angular coordinate
ρ = density
σ = surface tension or Stefan–Boltzmann constant
Φ = scattering phase function
Ω = solid angle

Subscripts and Superscripts

b = bottom
conv = convection
eff = effective
in = incoming
lv = liquid-void interface
L = liquid
m = metal
mz = mushy zone
n = number of a time step
o = outer
P = center of the control volume
rad = radiative
s = solid
t = top
W = finite volume to the left of the control volume

Introduction

THERE are several engineering applications that involve energy demand at a later period than its supply, which requires a thermal storage system. The choice of an appropriate storage system is most frequently between using a sensible heat storage material and phase change material (PCM). The two systems have been previously reviewed in the literature.[1,2] PCM systems have received extensive attention in the past and have been investigated for a variety of applications.[3–7] Experimental data for space power systems applications have been obtained for ground PCM systems[8] as well as thermal energy storage (TES) flight experiments conducted on Space Shuttles *Columbia* and *Endeavor*.[9] These efforts were part of the development of solar dynamic power systems in space and were provided for different canister design and PCM type.

Presented as Paper 98-1018 at the 36th AIAA Aerospace Sciences Meeting, Reno, NV, 12–15 January 1998; received 5 November 1998; revision received 27 October 1999; accepted for publication 10 December 1999.

*Postdoctoral Research Fellow. Member AIAA.
†Chair and Professor, Mechanical Engineering Department. Associate Fellow AIAA.
‡Power Systems Engineer, Power and Propulsion Office.

Table 1 Test canister design features: ground and space experiments

Feature	Ground experiments	Space experiments
Material of construction	Haynes Alloy 188	Haynes Alloy 188
Outer diameter/wall thickness	4.98/0.129 (cm)	6.96/0.102 (cm)
Inner diameter[a]/wall thickness[b]/rod diameter	2.07/0.261 (cm)/N/A[c]	3.81/0.102/3.59 (cm)
Length/side-wall thickness	2.43/0.091 (cm)	6.94/0.102 (cm)
PCM	LiF-20%CaF_2	TES-1 LiF, TES-2 LiF-20%CaF_2
PCM mass/total canister mass	53/137 (g)	TES-1 265/543 (g), TES-2 300/578 (g)
Cycle time (% time heating)	91.1 min (60%)	TES-1 131 min (58%), TES-2 159 min (58%)

[a]Cooling air tube. [b]Thickness of canister inner wall plus cooling air tube wall. [c]N/A, not applicable.

Several numerical studies have been conducted to utilize the available experimental data for both the ground testing[7,8] and the space TES-1 experiment[7,9] in order to provide a better understanding of the processes involved in the canister heat transfer. The motivation of this study is to enhance further the computational capabilities and physical understanding of the phenomena by including a proper modeling of the void that exists in the canister caused by the density difference between the solid and liquid phases. Furthermore, the radiation heat-transfer analyses, in both the void and the liquid PCM,[10] were improved by using a finite volume method.[11] In this paper a systematic approach has been taken for the modeling process. Predictions of temperature history were obtained and evaluated against the experimental data. One of these data sets was conducted at NASA John H. Glenn Research Center at Lewis Field (ground experiments[8]), and the other was part of the OAST-2 Hitchhiker payload on the Space Shuttle *Columbia* in early 1994 and Space Shuttle *Endeavor* in the summer of 1996 (space experiments[9]). The physical characteristics of the canisters used in the two experiments are given in Table 1.

The objective is to determine the temperature distribution in the canisters. Effects of natural convection in the liquid PCM, radiation in the void and the liquid PCM, and variable volume of the void on the temperature distribution will be examined.

Geometry and Boundary Conditions

In general, the temperature and phase distribution in cylindrical canisters can be nonaxisymmetric because of asymmetric boundary and/or initial conditions. Hence, the present computational model has been developed in a general three-dimensional cylindrical geometry. However, this work mainly focuses on the predictions of axisymmetric distributions, and the effects of three-dimensionality will be explained for a particular case of the TES-1 experiment.

Ground Experiments

The geometry of the ground experiments is shown in Fig. 1. The canister is filled with the eutectic mixture of LiF-20%CaF_2 with the melting point at 1040 K. The void is considered to be in the region adjacent to the top wall caused by the buoyancy force and consistent with the experimental observations when the canister was in the vertical position.[8] The top and the bottom walls of the canister are insulated. Heating is provided by a heater on the outside wall. The heat flux is axially uniform and periodic in time. The effective heating power, which is the difference of the heater power and the power of the radiative heat losses between the canister and the test chamber, was computed[8] and shown in Fig. 2. Cooling of the canister is provided by cooling air flowing in the inside tube. The output power to the air[7] is also provided on Fig. 2.

Space Experiments

The geometry of the space experiments is plotted in Fig. 3. Because the TES-1 and -2 experiments were performed in a microgravity environment, the location of the void is controlled by the surface tension rather than the gravity force. Because of the Marangoni effect that exists because of the temperature dependence of the surface tension coefficient, the void tends to be in the hottest region of the canister, that is, the outer lower corner in this problem.[9]

Again the top and the bottom sides of the canister are insulated. Heating is provided by a heater on the outside wall of the canister. Similar to the ground experiments, the effective heating power can be estimated[12] (Figs. 4 and 5 for TES-1 and -2, respectively).

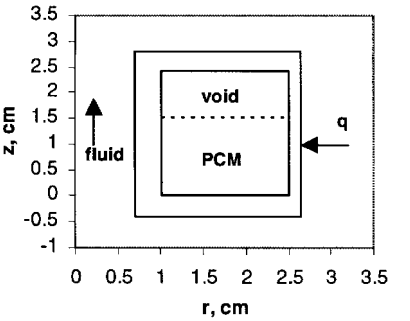

Fig. 1 Geometry of ground experiments.

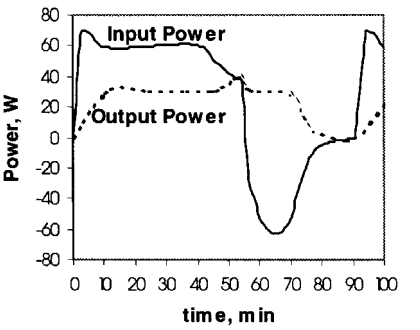

Fig. 2 Input and output power for ground experiments.

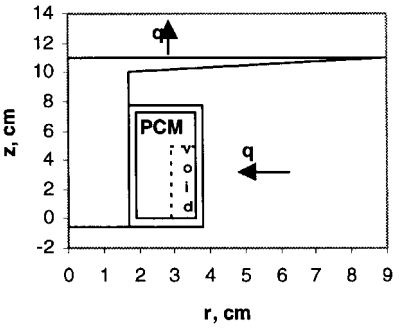

Fig. 3 Geometry of space experiments.

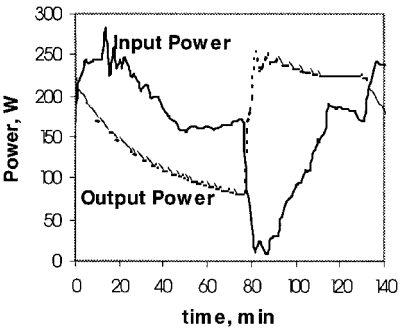

Fig. 4 Input and output power for space experiments: TES-1.

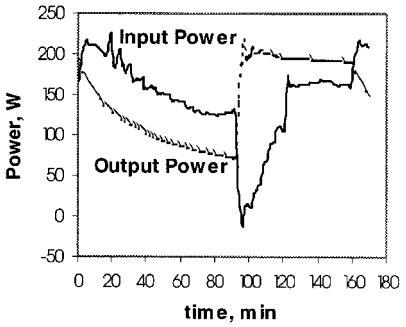

Fig. 5 Input and output power for space experiments: TES-2.

Cooling is done by radiation from the surface of a circular disk (radiator) attached to the canister via a conductor rod. The boundaries of the rod and the radiator are insulated except for the radiating surface of the radiator. The first test TES-1 used LiF as the PCM, whereas the second test TES-2 used the eutectic LiF-CaF_2.

Governing Equations

PCM, Walls, Conduction Rod, and Radiator

The enthalpy formulation of the heat-transfer equation is used. This approach has proved to be effective for problems with solid-liquid phase change.[4,13–15] The conservation of energy equation in this approach becomes[14]

$$\frac{\partial}{\partial t}(\rho e) + (\boldsymbol{v}\cdot\Delta)(\rho e) = \Delta\cdot(k\Delta T) - \Delta\cdot q_{\text{rad}} \tag{1}$$

This approach eliminates the need to introduce an infinitely large heat capacitance in the melting region to ensure the isothermal melting. The enthalpy is connected to the temperature via the constitutive equations as follows.

Solid PCM:

$$T_m + e/c_s, \qquad e < 0$$

Mushy PCM:

$$T = T_m, \qquad 0 \le e \le H_m$$

Liquid PCM:

$$T_m + (e - H_m)/c_L, \qquad H_m < e$$

Metal parts:

$$T_m + e/c_m, \qquad -\infty \le e \le \infty \tag{2}$$

Equation (2) indicates that the temperature stays constant and equal to the melting temperature in the so-called mushy zone, which can be viewed as a transition zone between the solid and the liquid phases.

The second term of Eq. (1) is a transport term, and it contains the velocity of the liquid phase. The velocity distribution in the liquid PCM is governed by the gravity and surface tension of the liquid-void interface. Determining this distribution is complicated and, most importantly, time consuming. Because we are interested mostly in the global heat transfer, the natural convection in the liquid PCM is modeled using the existing empirical correlations. The common approach is to estimate the enhancement of the value of the liquid PCM thermal conductivity such that

$$k_{L,\text{eff}} = Nuk_L \tag{3}$$

The Nusselt number has been estimated using a correlation for an isothermal vertical layer.[16] The effective conductivities of the solid PCM and the metal parts are equal to their normal values, the liquid effective conductivity is computed using Eq. (3), and the effective conductivity of the mushy PCM is treated as a linear function of the PCM quality $x_f = e/H_m$:

$$k_{\text{mz,eff}} = (1 - x_f)k_s + x_f k_{L,\text{eff}} \tag{4}$$

The liquid PCM (LiF) has been found[10] to be transparent to the thermal radiation for wavelengths $\le 5.5\mu$m and semitransparent for wavelengths $> 5.5\mu$m. The average Rossland absorption coefficient is virtually constant in the temperature interval of the interest (1000–1200 K) and equal to 0.84 cm^{-1} (Ref. 10). Because the low wavelength range has been excluded during the computations of the Rossland absorption coefficient,[10,12] both the transparent and the semitransparent models of the liquid PCM should be examined. In the former case the last term of Eq. (1) becomes zero because it can be shown that the divergence of the radiative heat flux is proportional to the absorption coefficient for a uniform medium. However, the radiative heat flux can be nonzero in the case of the transparent medium, although its divergence is zero. Therefore, this heat flux has been computed and used in the energy balance equations for the solid PCM and wall finite volumes adjacent to the liquid PCM layer.

Void

The void is assumed to be filled with the PCM. Because the mass of the vapor in the void is of order of 10^{-8} g (Ref. 4), the void is assumed to have negligible thermal capacity and absorption coefficient. Hence, the heat-transfer equation in the void is

$$\Delta\cdot(k\Delta T) = 0 \tag{5}$$

Similar to the liquid PCM model, the radiative heat flux in the void can be nonzero, although its divergence is zero because of the negligible absorption coefficient. Therefore, this heat flux has been computed and used in the energy balance equations of the PCM and walls finite volumes adjacent to the void.

The volume of the void is assumed to be varying according to the conservations of the PCM mass and energy during melting or solidification. The conservation of PCM mass can be written in the following form:

$$\int_{\text{PCM}} (\rho^{n+1} - \rho^n)\,\mathrm{d}V = 0 \tag{6}$$

The conservation of energy in the system can be written as[12]

$$\int_{\text{system}} [(\rho e)^{n+1} - (\rho e)^n]\,\mathrm{d}V + E_{\text{rad}} = E_{\text{in}} - E_o \tag{7}$$

Because the density of the liquid phase is smaller than that of the solid phase, the total mass of the PCM would reduce during melting and increase during solidification if the PCM volume were kept constant. An additional volume of PCM should be added to or subtracted from the domain to compensate for the mass loss or gain. In the present study the assumption is made that the change of mass during the phase change process occurs in the mushy zone.

The compensating PCM mass is uniformly added to or subtracted from the liquid PCM-void interface:

$$\Delta m_{\text{lv}} = -\Delta m_{\text{mz}} \tag{8}$$

The solid PCM-void interface is assumed to be immovable. Therefore, the density in the regions containing the solid-void interface remains constant.

During this procedure, there are cells in the computational domain that undergo a transition from the liquid PCM to the void. Because the void's thermal capacitance is zero and the liquid PCM thermal capacitance has a finite value, such transitions would cause a break of the energy balance. The additional energy of these transitions is interpreted as the convection energy of the flows caused by the void expansion/contraction:

$$E_{\text{conv}} = \int_{\rho^n = \rho_l,\ \rho^{n+1} < \rho_l} (e\rho)^n\,\mathrm{d}V - \int_{\rho^n < \rho_l,\ \rho^{n+1} = \rho_l} (e\rho)^{n+1}\,\mathrm{d}V \tag{9}$$

To compensate for this energy loss or gain, this energy is uniformly added to or subtracted from the energy of the volume containing the liquid PCM.

Hence, the procedure defined by Eqs. (8) and (9) is capable of predicting the void volume during the phase change process while maintaining the mass and energy balance. However, the shape of the void is governed by the surface tension forces[9,17] of the liquid-void interface and cannot be deduced from the procedure described

here. The present study was focused on analyzing the influence of the radiation heat transfer and the void size on the canister performance, and the surface tension forces were not included in the model.

Radiation Heat-Transfer Model

The finite volume method (FVM) developed by Chai and coworkers[11] has been used to compute the radiative heat flux. The equation of radiative transfer can be written in terms of the radiative intensity $I(\boldsymbol{r}, \boldsymbol{s})$ and the source function $S(\boldsymbol{r}, \boldsymbol{s})$[18]

$$\frac{\mathrm{d}I(\boldsymbol{r}, \boldsymbol{s})}{\mathrm{d}\boldsymbol{s}} = -\beta(\boldsymbol{r})I(\boldsymbol{r}, \boldsymbol{s}) + S(\boldsymbol{r}, \boldsymbol{s}) \tag{10}$$

$$S(\boldsymbol{r}, \boldsymbol{s}) = \alpha(\boldsymbol{r})I_b(\boldsymbol{r}) + \frac{\sigma(\boldsymbol{r})}{4\pi}\int_{4\pi} I(\boldsymbol{r}, \boldsymbol{s}')\Phi(\boldsymbol{s}', \boldsymbol{s})\,\mathrm{d}\Omega' \tag{11}$$

If Eq. (10) is solved subject to emissive boundary conditions,[11] then one can compute the radiative heat flux and its divergence via the equations

$$q(\boldsymbol{r}) = \int_{4\pi} I(\boldsymbol{r}, \boldsymbol{s})\boldsymbol{s}\,\mathrm{d}\Omega \tag{12}$$

$$\Delta \cdot q(\boldsymbol{r}) = \alpha\left(4\pi I_b(\boldsymbol{r}) - \int_{4\pi} I(\boldsymbol{r}, \boldsymbol{s})\right)\mathrm{d}\Omega \tag{13}$$

To solve Eq. (10) numerically, the coordinate space is discretized into finite volumes. Because the intensity I also depends on the angular direction, the angular space should be discretized as well. In the present method the angular space is divided into solid angles.

Integrating Eq. (10) over a control finite volume ΔV in the two-dimensional axisymmetric system and a control solid angle $\Delta\Omega^l$ and using the divergence theorem, we obtain

$$\sum_{i=1}^{4} I_i^l \Delta A_i \int_{\Delta\Omega^l} (\boldsymbol{s}^l \cdot n_i)\,\mathrm{d}\Omega^l = \left(-\beta_m^l I^l + S_m^l\right)\Delta V \Delta\Omega^l \tag{14}$$

the summation is performed over the four faces of the control volume. The modified extinction coefficient and the source function, respectively, are

$$\beta_m = \beta - \frac{\sigma}{4\pi}\Phi^{l,l}\Delta\Omega^l, \qquad S_m^l = \alpha I_b + \frac{\sigma}{4\pi}\sum_{l' \neq l}\Phi^{l',l}\Delta\Omega^{l'} I^{l'}$$

One can solve Eq. (14) for the intensity in the center P of the control volume:

$$I_P = \frac{(1 - \Delta\boldsymbol{r}/2\boldsymbol{r}_P)\Delta z D_{\mathrm{cr}}^l I_W^l + \Delta\boldsymbol{r} D_{\mathrm{cz}}^l I_S^l + S_{\mathrm{mP}}^l \Delta\boldsymbol{r}\Delta z\Delta\Omega^l}{(1 + \Delta\boldsymbol{r}/2\boldsymbol{r}_P)\Delta z D_{\mathrm{cr}}^l + \Delta\boldsymbol{r} D_{\mathrm{cz}}^l + \beta_{\mathrm{mP}}^l \Delta\boldsymbol{r}\Delta z\Delta\Omega^l} \tag{15}$$

Chai et al.[11] modified Eq. (15) by exponentially extrapolating the intensity at the neighboring nodes to the sides of the control surface ΔA. Their procedure increases the accuracy of the scheme and eliminates the possibility of a physically incorrect negative intensity. The resulting scheme[11] has been used to solve for the radiative intensity and the heat flux.

Boundary and Initial Conditions

Boundary Conditions

The following three boundary conditions in the experiments have been applied:

1) The heating boundary condition at the outside wall is

$$\boldsymbol{r} = \boldsymbol{r}_0\colon\ -k_m\frac{\partial T}{\partial \boldsymbol{r}} = q_{\mathrm{in}} \tag{16}$$

The function $q_{\mathrm{in}}(t)$ has been estimated for a full cycle of the ground experiments[8] as well as the space experiments[12] (TES-1 and -2) based on the power of the outside heater and the radiative heat transfer between the canister and the environment.

Equation (16) assumes an axisymmetric heat flux and, therefore, temperature distribution. An example of a nonaxisymmetric three-dimensional heat-flux distribution was considered for TES-1 only. In this case the following angular distribution of the heat flux was adopted:

$$q_{\mathrm{in}}(\theta) = (1.17\cos\theta + 0.63)q_0 \qquad \text{if} \quad 0 \le \theta \le \pi$$

$$q_{\mathrm{in}}(\theta) = 0.63q_0 \qquad \text{if} \quad \pi \le \theta \le 2\pi \tag{17}$$

2) The insulation boundary condition at the top and the bottom walls is

$$z = z_t, z_b\colon\ -k_m\frac{\partial T}{\partial z} = 0 \tag{18}$$

3) The cooling boundary conditions are different in each experiment.

a) Ground experiments are

$$\boldsymbol{r} = \boldsymbol{r}_i\colon\ -k_m\frac{\partial T}{\partial \boldsymbol{r}} = h[T - T_f(z)] \tag{19}$$

The cooling air temperature is determined by utilizing the time-dependent inlet profile[8] and assuming a linear temperature distribution in the z direction.

b) Space experiments are

$$z = z_{\mathrm{rad}}\colon\ -k_m\frac{\partial T}{\partial z} = \sigma_{\varepsilon_m}\left(T^4 - T_{\mathrm{sink}}^4\right) \tag{20}$$

T_{sink} is the temperature of the surrounding.

Initial Condition

The system is assumed to initially be at a uniform temperature in both experiments. The initial temperature is 922 K in the ground experiments and 283 K in the space experiments.

Numerical Method

The simple explicit method is used to solve Eq. (1). In contrast with the parabolic PCM heat-transfer equation, the heat-transfer equation in the void [Eq. 5] is elliptic. Therefore, a simple explicit method cannot be used, and the successive overrelaxation by lines procedure for the Laplace equation[19] has been used. The radiative heat flux was computed using the FVM.[11] The value of the divergence of the radiative heat flux in the liquid PCM was substituted in the energy balance [Eq. (1)]. In addition, the value of the radiative heat flux on the void and liquid boundaries was used as a boundary condition for the PCM and wall regions adjacent to the boundaries.

The radial and axial grid in the numerical simulations was chosen to be approximately 20 grid points per centimeter in the PCM. This resolution provides convergence of the numerical solution with a tolerance of less than 0.001. Coarser grid resolution was selected in the circumferential direction for the three-dimensional simulations as the primary heat-transfer path is in the radial and axial directions. About 5 grid points per centimeter, or 16 per circle, were used in the circumferential grid. In the radiative heat-flux calculations a grid containing 32 finite solid angles (4 azimuthal×8 polar angles) was proven to be sufficient to provide an accurate solution. Finally, time-step values of 0.02s for the ground experiments and 0.08s for the space experiments were chosen such that the stability criteria for the explicit scheme were satisfied.[4]

Results and Discussion

Most computations were performed for the two-dimensional axisymmetric geometry. Effects of three-dimensionality were also considered and will be described next. The objective of the numerical simulations was to analyze the influence of the convective and radiative heat-transfer modes, as well as the void volume and nonaxisymmetric boundary conditions, on the canister performance.

All numerical simulations consisted of two parts. First, computations were performed with a void of a constant volume, i.e., with the liquid and solid densities equal to each other and to the average density $(\rho_l + \rho_s)/2$. In the second part the solid and the liquid densities were different and, therefore, the void volume was varying during the phase change process.

The following four cases were analyzed in both parts: case 1, neither the void nor the liquid PCM are transparent to thermal radiation; case 2, the void is transparent, but the liquid PCM is not; case 3, both the void and liquid PCM are transparent; case 4, the void is transparent, and the liquid is semitransparent with the absorption coefficient equal to 0.83 cm^{-1} for LiF and 0.84 cm^{-1} for LiF-20%CaF_2.

Ground Experiment

Figure 6 shows the comparison of the outside wall temperature predicted by the numerical solution for the four radiation cases with the experimental data.[8] The numerical solution captures very closely the important features of the temperature history: the slope during the subcooled solid heating (0–15 min) and cooling (65–91 min); the point of the onset of melting (15 min); the temperature arrest during melting (15–40 min) and solidification (55–65 min); and overheated liquid heating and cooling (40–55 min).

Effect of Natural Convection in Liquid PCM

Figure 7 shows the effect of natural convection on the outside wall temperature. The wall temperature is lower when convection is present in the time intervals when liquid exists in the canister. Thus, convective heat flux reduces the effective canister thermal resistance and lowers temperature gradients.

Convection has almost no effect during the freezing thermal arrest (55–65 min). Because of negative heat fluxes absorbed by both the inside and outside walls (Fig. 2), two layers of solid PCM at the melting temperature are formed at the inside and outside walls. The liquid PCM is trapped between these layers and brought to a uniform melting temperature, which brings the Nusselt number to 1.

Effect of Radiation in the Void

As seen from the comparison of temperature histories in cases 1 and 2 in Fig. 6, inclusion of radiation in the void lowers the outside wall temperature by about 5 K. Because radiation in the void is an additional heat-transfer mechanism in the canister, it lowers the effective canister thermal resistance and, therefore, temperature gradients.

Effect of Radiation in the Liquid PCM

Similar to the radiation in the void, radiation in the liquid PCM lowers the canister thermal resistance and temperature gradients. Its effect is however more pronounced than that of radiation in the void as seen from the comparison of outside wall temperatures in cases 3 and 4 with case 2. The maximum temperature in case 3 is lower than that in case 2 by about 15 K compared to the 5 K improvement in the case of radiation in the void only.

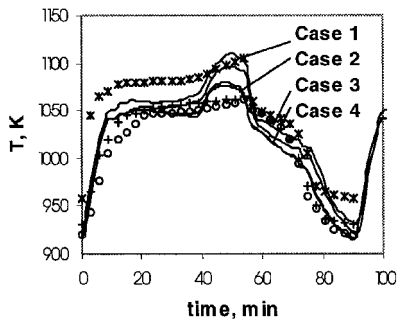

Fig. 6 Experimental (symbols) and computational canister outside wall temperature data: ground experiments, stationary void.

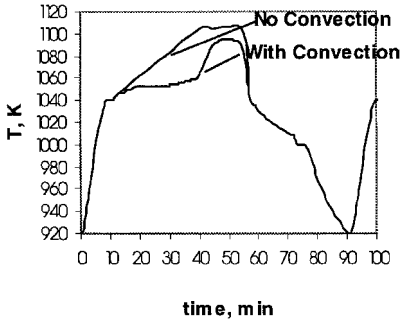

Fig. 7 Canister outside wall temperature with and without natural convection: ground experiments, case 2, stationary void.

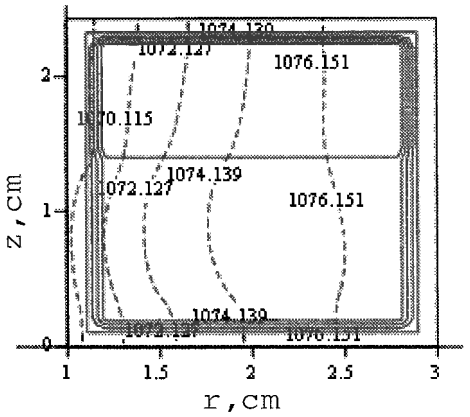

Fig. 8 Canister temperature (– – –) and density (——) contours: ground experiments, case 4, stationary void.

As seen in Fig. 8, radial gradients dominate in the temperature distribution in the canister. The void is located in the upper portion of the canister and faces only about 30% of outside and inside wall surface areas. Hence, the radiative heat transfer through the void, which takes place mostly in the radial direction from the outside to the inside wall, has only a minor effect on the overall heat transfer. On the other hand, the liquid PCM layer faces about 70% of the outside and inside wall surface areas and, therefore, significantly affects the overall canister heat transfer. The void represents the location of two hot spots, i.e., local nonuniformities in the temperature distribution. These nonuniformities generally cause local thermal stresses in the canister walls.

The effect of absorption in the liquid PCM is seen from the comparison of the temperature histories in cases 3 and 4 on Fig. 6. When the liquid absorbs a portion of incoming energy, it results in lower temperature in the canister. This effect is not significant because of a low canister optical thickness $\tau = \alpha(r_0 - r_i) = 0.8946 < 1$.

Effect of Variable Void Volume

The same four cases, as just described, were run while different values were set for the liquid and solid phases, thus allowing the void volume to change during the phase change process. In general, computations showed little difference with the stationary void computations. This is an indication that the convective heat transfer caused by the flows induced by changing void size has an insignificant effect. This result has been confirmed previously by many authors.[14,20,21] When there is a difference in the temperature histories, it can be attributed to the specifics of the void configuration.

To illustrate the effect of a moving void in ground experiments, let us compare the temperature histories in case 4 when the void is stationary and moving (Fig. 9). The wall temperature in the situation when the void is moving is lower than when the void is stationary. Comparison of temperature and density contours in Figs. 8 and 10 shows that the void loses its contact with the outside wall when it is subject to a change of size caused by the phase change in the PCM. The wall temperature decreased because of the higher conductivity of the PCM than the void. Therefore, a quenching effect takes place, which results in the lower temperatures of the outside wall. A similar effect takes place in other radiation cases as well.

Space Experiments

Cases 1 through 4 were again considered. Figures 11 and 12 show the outside wall temperature predictions for TES-1 and -2, respectively. The same features as in the ground experiments are observed here: subcooled solid heating and cooling, overheated liquid heating and cooling, and thermal arrest during melting and solidification. In

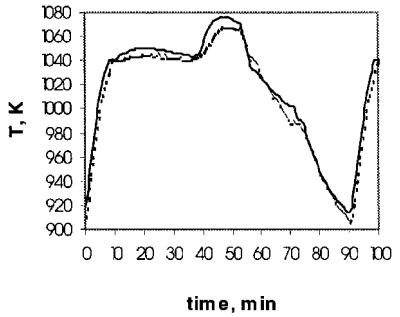

Fig. 9 Canister outside wall temperature with a stationary void (——) and variable volume void (– – –): ground experiments, case 4.

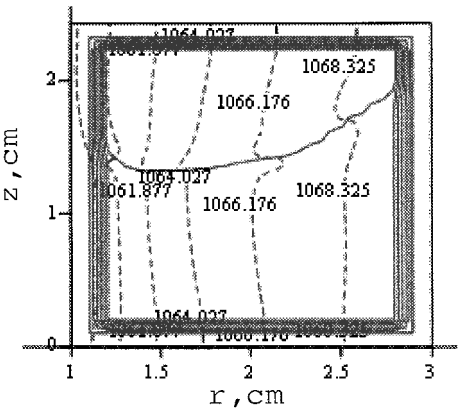

Fig. 10 Canister temperature (– – –) and density (——) contours: ground experiments, case 4, variable volume void.

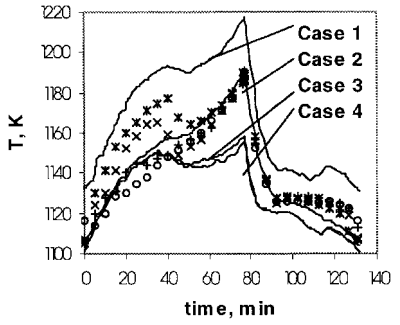

Fig. 11 Experimental (symbols) and computational canister outside wall temperature data: space experiments, TES-1, stationary void.

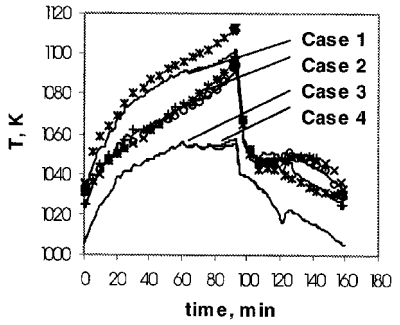

Fig. 12 Experimental (symbols) and computational canister outside wall temperature data: space experiments, TES-2, stationary void.

general the comparison with the experimental flight data is satisfactory. Cases 3 and 4 did not compare well with the data because the input and output power were estimated with the assumption of no radiation heat transfer in the liquid PCM.[12]

Effect of Radiation in the Void

The presence of radiation in the void has a more significant effect in the space experiments than in the ground experiments. The reason for that is a larger surface area of the void is exposed to the incoming

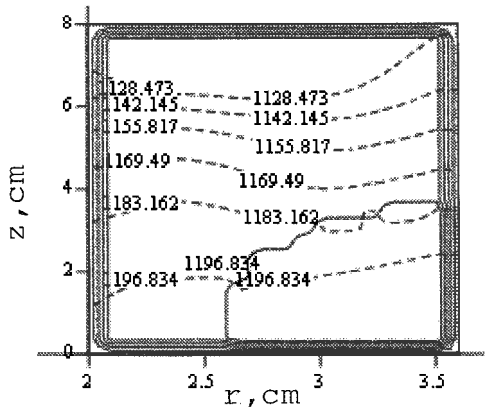

Fig. 13 Canister temperature (– – –) and density (——) contours: space experiments, TES-1, case 4, stationary void.

heat transfer. The effect of radiation in the void on the temperature distribution in the canister is seen in Figs. 11 and 12. As expected, the outside wall temperature is significantly lower in the presence of thermal radiation in the void. This improvement is about 30 K compared to 5 K for the ground experiments. The improvement is more significant in TES-1 than in TES-2, because a larger void exists in TES-1. The size of the void is proportional to the density difference between the solid and liquid PCM. This density difference is equal to 0.75 g/cm^3 for TES-1 compared to 0.4 g/cm^3 for TES-2. The temperature difference between the boundaries is higher for a larger void. This results in an improved radiative heat-transfer rate. Computations showed that void radiative heat fluxes in TES-1 were higher than those in TES-2 by about 20-30%.

The void is again the location of a hot spot in the canister. As seen in Fig. 13, there is only one hot spot (compared to two in the ground experiments) adjacent to the canister outside wall.

Effects of Radiation in the Liquid PCM

During the heating part of the cycle, the PCM starts to melt first in the region close to the canister bottom wall because of the significant z component of the heat flux and presence of the void adjacent to the outside wall. Therefore the solid-liquid interface is close to being perpendicular to the z axis as seen in Fig. 13. As more liquid PCM is formed during the heating part of the cycle, the interface moves up along the z axis. Because the interface is located between the inner wall and the void in the start of the heating portion of the cycle, the liquid PCM layer is not facing the outside wall heat flux.

Computations showed that the radiation through the liquid PCM, whether absorbing or not, does not have an effect as important as the radiation through the void. This is obvious from the comparison of the temperature histories for cases 3 and 4 with that in case 2 in Figs. 11 and 12. The reason for this phenomenon is the configuration of the liquid PCM layer just described, which results in the heat mostly transferred through the void rather than the liquid in the beginning and the end of the heating-cooling cycle.

The effect of the radiation through the liquid PCM becomes more important when more liquid is formed and the height of the liquid layer exceeds the height of the void. This event happens at about 40 min of the canister cycle time for both TES-1 and TES-2 as seen in Figs. 11 and 12. The improvement of the canister temperature caused by the radiation in the liquid PCM becomes more significant.

Effect of Variable Void Volume

The same four radiation cases were considered for TES-1 and TES-2 in a situation when the void was changing in size during the phase change process. Similar to the stationary void simulations, the radiation in the void lowers the temperature of the canister outside walls, and the radiation in the liquid PCM further increases this effect. The distinctive difference from the stationary void simulations is that during the time period when the liquid PCM is present in the canister the radiation in liquid PCM has a larger effect than the radiation in the void. This difference can be explained by the fact that during this time the void becomes smaller than the average

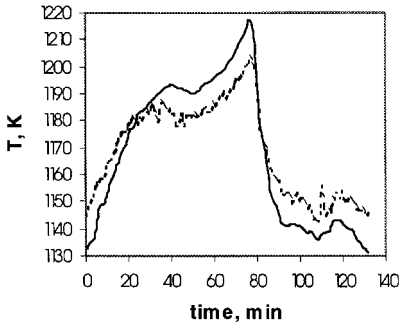

Fig. 14 Canister outside wall temperature with a stationary void (——) and variable volume void (– – –): space experiments, TES-1, case 1.

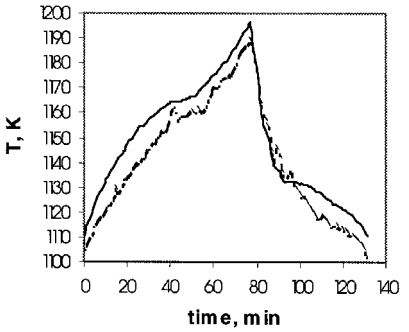

Fig. 15 Canister outside wall temperature with a stationary void (——) and variable volume void (– – –): space experiments, TES-1, case 2.

size and the liquid PCM volume is larger than in the stationary void simulations. Therefore, the total radiative energy passing through the void is larger in the stationary void simulations, and the total radiative energy passing through the liquid PCM is larger in the moving void simulations.

The effect of a transient void depends on whether radiation in the void is involved or not. This effect is illustrated in cases 1 and 2 for TES-1. The comparison of temperature histories in each individual case with respect to radiation is given in Figs. 14 and 15.

When the radiation is not present in the void nor in the liquid PCM, the outside wall temperature in the moving void simulations is higher than that in the stationary void simulations when the void is larger than the average size (see Fig. 14; time of 0–20 min and 80–131 min). When the void is smaller than average, then the temperature in the canister with a moving void is lower than that in the canister with a stationary void because the effective conductivity of the void without radiation, consisting only of the void molecular conductivity, is strictly proportional to the void volume.

The situation is different when the radiation in the void is included. The effective conductivity is now the sum of the molecular and radiative parts. The void radiative heat flux is higher for a larger void because of a higher temperature difference between the boundaries of the void. Hence, the void effective radiative conductivity may increase for a larger void volume and compensate the decrease in the canister molecular conductivity. Accordingly, we obtain lower temperatures in the changing size void model than in the stationary void model, as shown in Fig. 15.

If the liquid PCM is also transparent to thermal radiation, then the variable volume of the void has the same effect as in case 1. The combined void and liquid region is the same whether the void is changing its volume or not. Therefore, the effective radiative conductivity remains unchanged. However, the molecular void conductivity depends on the volume, producing higher temperatures when the void is larger than the average and lower temperature when the void is smaller than the average.

Temperature and density contours for TES-1 are shown in Fig. 16. The observed void shape would probably be significantly altered if the liquid-void surface tension were involved. The void's size is smaller than that in the stationary void computations (Fig. 13)

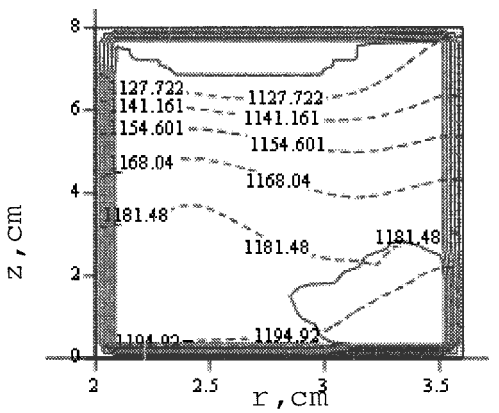

Fig. 16 Canister temperature (– – –) and density (——) contours: space experiments, TES-1, case 4, variable volume void.

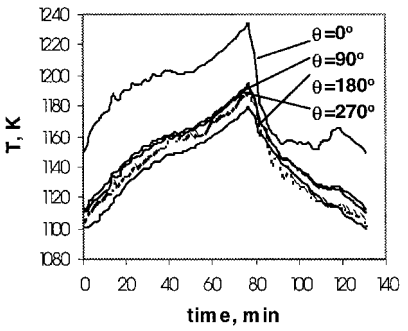

Fig. 17 Canister outside wall temperature predictions by three-dimensional model (——) and axisymmetric model (– – –): space experiments, TES-1, case 2, variable volume void.

because a significant part of the PCM is melted and requires a larger volume to satisfy the mass balance.

Three-Dimensional Effects

The heat-flux distribution described by Eq. (16) was used for three-dimensional computations. The overall heat inputs in both axisymmetric and three-dimensional cases are equal to each other. Only simulations for the space experiments in case 2 with a transient void were performed to show effects of the angular dependence of the outside wall flux.

The comparison of the three-dimensional solutions with the experimental data and the axisymmetric case is shown on Fig. 17. The temperature at the location $\theta = 0$ is always higher than that in the axisymmetric case because of a higher heat flux at that location compared to the axisymmetric heat flux. The temperatures at $\theta = \pi/2$ and $3\pi/2$ are higher than that at $\theta = \pi$, although the heat fluxes are equal to each other. This thermal characteristics are a consequence of the existence of considerable circumferential heat fluxes in the canister walls and PCM. Because the heat-flux distribution is symmetric relative to the line $x = 0$ in the (x, y) plane, $q(\theta) = q(2\pi - \theta)$; the temperature distribution is also symmetric relative to the same line.

The temperature and density contours in the (x, y) plane (Fig. 18) confirm that not only the temperature distribution is nonaxisymmetric, but so is the density distribution. For instance, Fig. 18 shows that the void is nonexistent at $\theta = 0$, but appears at approximately 10 deg and grows in size until it reaches its maximum size at 180 deg. The solid distribution is also nonaxisymmetric. The rate of melting of the solid PCM depends on the local heat-transfer distribution. Because of the heat-flux distribution, the local concentration of the solid PCM is minimal at angular location $\theta = 0$ and maximal at $\theta = 180$ deg.

Therefore, the asymmetry in the temperature distribution creates an asymmetry in the void distribution. During the onset of melting, the liquid PCM starts to form first in the hottest region, which is located near the outside wall at $\theta = 0$. Because the solid-void is immovable, the size and shape of the void in regions containing

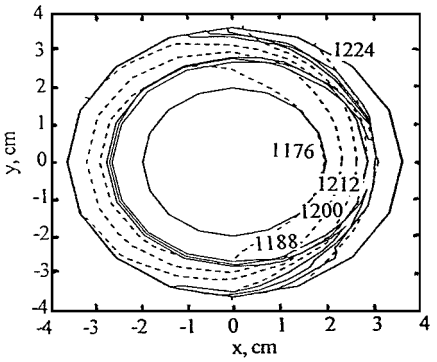

Fig. 18 Canister temperature (- - -) and density (——) contours: space experiments, TES-1, case 2, variable volume void, view from above, (x, y) plane, $z = L/4$.

solid remain unchanged. On the other hand, the liquid-void interface is moving and shrinking the void in the regions containing liquid PCM. Thus the void is smallest in the regions that melt first (and solidify last), i.e., the hottest regions. Unfortunately, this result contradicts the observations that showed that the void tends to be in the hottest regions. This phenomenon can be explained by the influence of the Marangoni flow on the liquid-void interface.[17] Because surface tension flows have been excluded from the transient analysis in the present study, this effect is not seen in the computational results.

Conclusions

Two-dimensional axisymmetric and three-dimensional computational models of cylindrical phase change thermal energy storage canisters were developed. Data from ground and space experiments were analyzed.

The strength of the models is in the fact that they include two features that were often omitted in previous studies, namely the radiative heat transfer in the void and the liquid PCM and a void model that accounts for the void volume change during the phase change. Although the models were developed in the cylindrical system of coordinates, Cartesian and spherical versions can be developed using the same approach.

This study showed that the void is a location of hot spots in the canister. A smaller void size results in a higher effective canister conductivity and, therefore, lower temperatures. When the void is changing in size, it can create a quenching effect in the canister walls, i.e., a larger area of contact between the liquid PCM and canister walls, which results in lower temperatures.

Inclusion of the radiative heat flux in the void and the liquid PCM reduces the overall canister thermal resistance and results in decreasing the canister-wall temperature. Absorption in the liquid PCM has a negligible effect on the temperature distribution in canisters because of the small optical length of the liquid layer.

Computations showed that surface-tension-driven and Marangoni-type flows should be considered in future investigations. Inclusion of these flows would improve capabilities to predict the shape and location of the void, which proved to be a vital part in accurate computations of the canister behavior.

Specific conclusions for the ground experiments are that convection heat transfer is equally important to that of the radiation heat transfer and that radiation heat transfer in the liquid is found to be more significant than that in the void. Including the radiation heat transfer in the liquid resulted in lower temperatures (about 15 K). In addition, a transient void creates a quenching effect, when the temperature of the outside wall in simulations with a moving void is lower than in stationary void simulations.

For space experiments radiation transfer in the void is found to be more significant than that in the liquid (exactly the opposite of the ground experiments). Accordingly, the location and size of the void affect the performance considerably. In addition, including the radiation heat transfer in the void resulted in lower temperatures (about 30 K). Moreover, an asymmetry in the heat flux creates asymmetries not only in temperature distribution, but also in the void distribution. The void tends to be smaller in hotter regions.

Acknowledgments

The authors appreciate the support of NASA Grant NAG3-1756 and Ohio Supercomputer Center Grant PFS187.

References

[1]Beasley, D. E., and Clark, J. A., "Transient Response of a Packed Bed for Thermal Energy Storage," *International Journal of Heat and Mass Transfer*, Vol. 27, No. 9, 1984, pp. 1659–1669.

[2]Yao, L. S., and Prusa, J., "Melting and Freezing," *Advances in Heat Transfer*, Vol. 19, 1989, pp. 1–95.

[3]Beasley, D. E., Ramanarayanan, C., and Torab, H., "Thermal Response of Packed Bed of Spheres Containing a Phase-Change Material," *International Journal of Energy Research*, Vol. 13, 1989, pp. 253–265.

[4]Kerslake, T. W., and Ibrahim, M. B., "Analysis of Thermal Energy Storage Material with Change-of-Phase Volumetric Effects," *Journal of Solar Energy Engineering*, Vol. 115, No. 1, 1993, pp. 22–31.

[5]El-sayed, A. O., "Experimental and Numerical Investigations of the Melting Phenomenon of Encapsulated Phase Change Material in Horizontal Cylindrical Annuli," Ph.D. Dissertation, Power and Technology Engineering, Warsaw Univ. of Technology, Warsaw, Poland, 1995.

[6]Adebiyi, G. A., "A Second-Law Study on Packed Bed Energy Storage Systems Utilizing Phase-Change Materials," *Journal of Solar Energy Engineering*, Vol. 113, No. 3, 1991, pp. 146–156.

[7]Ibrahim, M. B., Kerslake, T. W., Sokolov, P. A., and Tolbert, C., "Experimental and Computational Investigations of Phase Change Thermal Energy Storage Canisters," *Proceedings of the Sixth International Congress on Fluid Dynamics and Propulsion*, edited by R. Mankbadi et al., Vol. 1, Cairo Univ. Press, Cairo, 1996, pp. 55–64.

[8]Kerslake, T. W., "Experiments with Phase Change Thermal Energy Storage Canisters for Space Station Freedom," *26th Intersociety Energy Conversion Engineering Conference*, Vol. 1, American Nuclear Society, La Grange Park, IL, 1991, pp. 248–261.

[9]Namkoong, D., Jacqmin, D., and Szaniszlo, A., "Effect of Microgravity on Material Undergoing Melting-Freezing—the TES Experiment," AIAA Paper 95-0614, Jan. 1995.

[10]Wichner, R. P., "Thermal Radiation Transfer Through LiF," DOE, Interagency Agreement No. 1819-1819-A, Martin Marietta Energy Systems, Inc., Dec. 1987.

[11]Chai, J. C., Lee, H. S., and Patanker, S. V., "Finite Volume Method for Radiation Heat Transfer," *Journal of Thermophysics and Heat Transfer*, Vol. 8, No. 3, 1994, pp. 419–425.

[12]Sokolov, P. A., "Computational Heat Transfer Modeling of Thermal Energy Storage Canisters," Ph.D. Dissertation, Mechanical Engineering Dept., Cleveland State Univ. Cleveland, OH, Aug. 1997.

[13]Solomon, A. D., and Wilson, R. L., "The Development of a Simulation Code for a Latent Heat Thermal Energy Storage System in a Space Station," Oak Ridge National Lab., TM-6213, Oak Ridge, TN, 1986.

[14]Alexiades, V., and Solomon, A. D., *Mathematical Modeling of Solid-Liquid Phase Change,* Hemisphere, New York, 1993, pp. 242–260.

[15]Brent, A. P., Voller, V. R., and Reid, R. J., "Enthalpy-Porosity Technique for Modeling Convection-Diffusion Phase Change," *Numerical Heat Transfer*, Vol. 13, No. 3, 1988, pp. 297–318.

[16]Özisk, M. N., *Heat Transfer: A Basic Approach*, McGraw–Hill, New York, 1985, pp. 452–455.

[17]Morris, D. G., Foote, J. P., and Olszewski, M., "Development of Encapsulated Lithium Hydrate Thermal Energy Storage for Space Power Systems," Oak Ridge National Lab., TM-10413, Oak Ridge, TN, 1987.

[18]Modest, M. F., *Radiative Heat Transfer*, McGraw–Hill, New York, 1993, p. 575.

[19]Anderson, D. A., Tannehill, J. C., and Pletcher, R. H., *Computational Fluid Mechanics and Heat Transfer*, Hemisphere, New York, 1984, p. 134.

[20]Prusa, J., and Yao, L. S., "Effects of Density Change and Subcooling on the Melting of a Solid Around a Horizontal Heated Cylinder," *Journal of Fluid Mechanics*, Vol. 155, 1985, pp. 193–212.

[21]Shansundar, N., and Sparrow, E. M., "Effect of Density Change on Multidimensional Conduction Phase Change," *Journal of Heat Transfer*, Vol. 98, No. 4, 1976, pp. 550–557.

M. Torres
Associate Editor